ISSN: 2472-3703 DOI: 10.6911/WSRJ.202601_12(1).0003

Performance Comparative Analysis and Structural Optimization of Split Mechanical Seals for Pumps

Junliang Zhang, Guanglei Zeng, Heshun Wang *, Weibing Zhu

School of Mechanical Engineering, Xihua University, Chengdu, Sichuan 610039, China

*Corresponding author: Heshun Wang (Email: wangheshun@mail.xhu.edu.cn)

Abstract

This paper focuses on the sealing performance of split mechanical seals used in pumps, proposing a new split seal structure with the sealing ring and support component installed at a 90° offset, and conducting a comparative performance study against traditional coplanar arrangements. The research establishes a 3D numerical model, combining ANSYS numerical simulation with orthogonal experimental methods to systematically analyze the impact of the gap between the end face and split face on leakage. The results show that the new design exhibits superior sealing performance under various gap conditions. Furthermore, through range and variance analysis, the significant order of the impact of each structural parameter on leakage was determined, optimizing a combination of structural parameters that achieved the best sealing performance, significantly reducing leakage, and providing a theoretical basis and reference for the structural design and performance improvement of split mechanical seals.

Keywords

Split mechanical seal; Numerical analysis; Sealing performance; Orthogonal test.

1. INTRODUCTION

Compared to conventional mechanical seals, the split mechanical seal is characterized by its core structural feature: the sealing assembly is split into two or more segments. This innovative design enables installation at the shaft end without the need to dismantle bearings, couplings, or adjacent components, thereby simplifying the replacement process, reducing downtime, and significantly improving maintenance efficiency for continuously operating equipment. This study focuses on a split mechanical seal system for pumps. Building upon the conventional mechanical seal structure, it innovatively proposes a novel split configuration where the seal ring and its support are installed with a 90° offset. A systematic investigation of its sealing performance is conducted.

In recent years, scholars at home and abroad have conducted systematic research in the field of split mechanical seals. Nagai Yataro et al [1] proposed a split ring design based on a pre-grooved support ring and an embedded O-ring. Radosav J J et al [2] developed a split seal structure consisting of arc-shaped ring segments and a two-piece bracket, while Bessette et al. [3] innovatively proposed a fully split cartridge mechanical seal design. Reagan [4] further improved the alignment technology for sealing rings, using special fixtures to ensure installation accuracy. In 2007, Giard [5] invented a composite split seal device, and Boyson [6] conducted an in-depth study on the reliability of split seals in centrifugal fluid devices, pointing out that nonlinear deformation and stress distribution under high sealing pressure are key challenges. Ma Weidong [7] was the first to develop split mechanical seals for large reactors and

ISSN: 2472-3703 DOI: 10.6911/WSRJ.202601_12(1).0003

pumps. Li Zhenhuan et al. [8] and Shao Jiaxing et al. [9] explored the structural characteristics and engineering applications of split seals for reactors, respectively. Zhang Yuan et al. [10] verified the feasibility of split seals for chlorination reactors through theoretical analysis and numerical simulation. Chen Bifeng [11] optimized the stress distribution of the sealing ring using the finite element method. Wang Hongqun et al. [12] improved the O-ring design to enhance sealing performance. Tao Kai et al. [13] used ANSYS to simulate the influence of preload, medium pressure, and other factors on the sealing performance of split surfaces. Feng Feifei et al. [14] and Hu Qiong et al. [15] systematically reviewed the research progress on split seals, pointing out that the temperature field of the end face, deformation mechanisms, and leakage models are key areas for future research. Liang Xiao et al. [16] proposed an optimization scheme for split seals in petrochemical stirring reactors based on failure analysis. These research findings provide a theoretical foundation for this article.

2. SPLIT MECHANICAL SEAL STRUCTURE

Similar to conventional mechanical seals, a split mechanical seal primarily consists of a face sealing pair, elastic elements, secondary seals, drive components, fasteners, and anti-rotation components. The sole distinction lies in the fact that, based on the standard mechanical seal structure, the seal rings in a split mechanical seal are completely split into two halves. The geometric model is shown in Figure 1, where the left side represents the rotating ring and the right side represents the static ring.

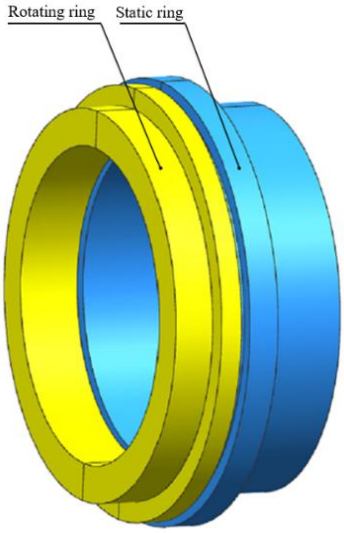

Figure 1. Geometric model of split seal ring

The novel split mechanical seal structure proposed in this paper, compared to traditional co-planar layout schemes, features a 90° arc-shaped guide groove at the rear of the static ring seat. This enables angular adjustment through a pin-and-groove matching mechanism: during assembly, the guide pin drives the static ring to rotate along the arc groove until the preset angular position is reached, after which an anti-rotation pin is inserted to achieve circumferential positioning. The design of this angular offset mechanism is illustrated in Figure 2.

ISSN: 2472-3703 DOI: 10.6911/WSRJ.202601_12(1).0003

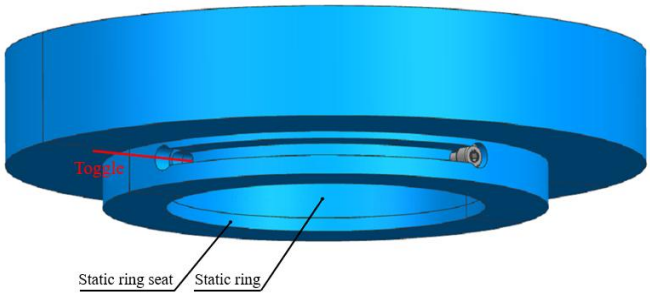

Figure 2. Angular misalignment schematic

3. NUMERICAL MODEL OF SPLIT MECHANICAL SEALS

3.1. Seal Ring Parameters and Analysis Model

The main dimensions of the sealing ring are shown in Figure 3, and the dimensional parameters are listed in Table 1.

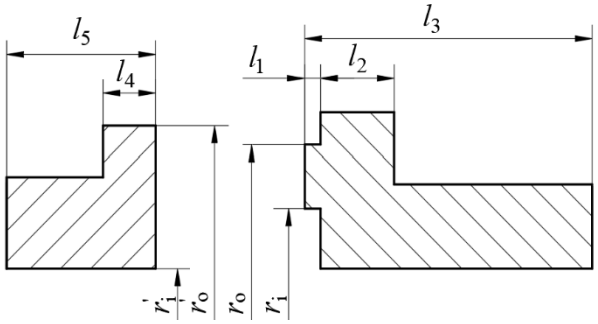

Figure 3. Main dimensions of sealing ring

Table 1. Seal ring geometry parameters

Parameter	Value
rotating ring face inner diameter r_i' /mm	22
rotating ring face outer diameter r_o' /mm	29.6
static ring face inner diameter r_i /mm	25
static ring face outer diameter r_o /mm	28.55
rotating ring rib thickness l_4 /mm	2~4
rotating ring axial thickness l_5 /mm	9
static ring face crown height l_1 /mm	1
static ring rib thickness l_2 /mm	3.2~5.2
static ring axial thickness l_3 /mm	16

This study used 3D software to establish comparative analysis models of two types of split mechanical seals. After reasonable simplification, both models consist of a split rotating ring, a static ring, and a static ring seat, with the specific geometric configuration shown in Figure 4. The key difference between the two models lies in the circumferential positional relationship between the static ring and the static ring seat: in Option 1, the split faces are aligned, while in Option 2, the split faces are circumferentially offset by 90°.

ISSN: 2472-3703 DOI: 10.6911/WSRJ.202601_12(1).0003

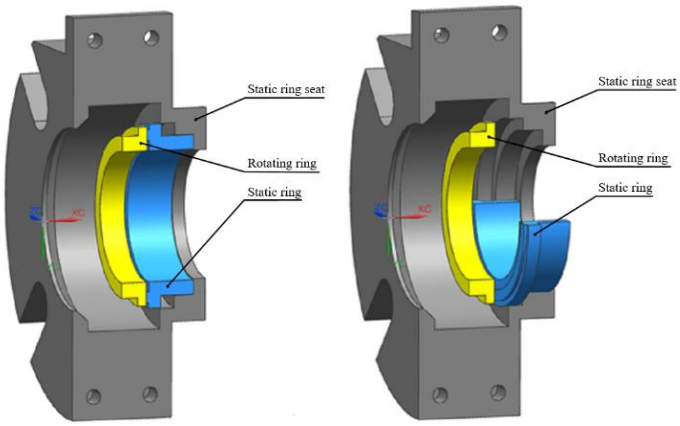

(a) Option 1 (b) Option 2

Figure 4. Model Schematic

3.2. Mesh Division and Independence Verification

After completing the geometric modeling using 3D modeling software, based on the differences in the geometric features of the components: hexahedral mesh discretization is applied to the structurally regular rotating and stationary rings, while tetrahedral mesh discretization is used for the structurally complex stationary ring seat. The final meshing results are shown in Figure 5. Based on the results of the thermo-structural coupled analysis, mesh independence is verified by monitoring the convergence of the maximum total deformation of the sealing ring with changes in mesh density: when the number of mesh elements increases to 147,640 (with 721,510 nodes), the maximum total deformations of the rotating and stationary rings are 0.0039604 mm and 0.0042843 mm, respectively. Further mesh refinement leads to stabilized deformation maxima, indicating that mesh independence is achieved. Therefore, this mesh configuration is adopted for subsequent analyses.

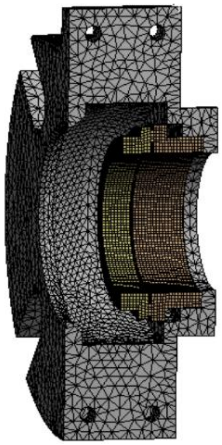

Figure 5. Schematic diagram of grid division

3.3. Computational Domain Setup

(1) End-face liquid film model

Based on the results of the thermo-structural coupled analysis, the sealing end face exhibits circumferential wave-like deformation characteristics under thermal-mechanical coupling. To accurately reconstruct the end face liquid film under operating conditions, this study uses the Fourier series expansion method to fit the axial deformation data of the inner and outer diameters of the seal ring, obtaining the end face profile curve. The fitting parameter equations for the two design schemes are as follows:

ISSN: 2472-3703 DOI: 10.6911/WSRJ.202601_12(1).0003

Option 1:

Outer diameter parameter equation:

$$\begin{aligned} X(\theta)&=28.55\cos(\theta) \\ Y(\theta)&=28.55\sin(\theta) \\ Z(\theta)&=0.6457+0.0164\cos(2\theta) \end{aligned} \tag{1}$$

Inner diameter parameter equation:

$$\begin{aligned} X(\theta)&=25\cos(\theta) \\ Y(\theta)&=25\sin(\theta) \\ Z(\theta)&=0.8123+0.0064\cos(2\theta)-0.0021\sin(2\theta) \end{aligned} \tag{2}$$

Option 2:

Outer diameter parameter equation:

$$\begin{aligned} X(\theta)&=28.55\cos(\theta) \\ Y(\theta)&=28.55\sin(\theta) \\ Z(\theta)&=0.6555+0.0165\cos(2\theta) \end{aligned} \tag{3}$$

Inner diameter parameter equation:

$$\begin{aligned} X(\theta)&=25\cos(\theta) \\ Y(\theta)&=25\sin(\theta) \\ Z(\theta)&=0.8310+0.01356\cos(2\theta) \end{aligned} \tag{4}$$

Based on the end-face profile curve obtained from fitting, a complete liquid film geometric model is established. Considering the axially symmetrical characteristic of the liquid film, half of the liquid film model is selected for numerical analysis to improve computational efficiency. Figure 6 shows the final three-dimensional computational domain model of the liquid film.

(a) Option 1 (b) Option 2

Figure 6. Schematic diagram of the calculation model of the liquid film on the end face

(2) Liquid Film Model for Split Faces

Similarly, the circumferential deformation of the seal ring split face is extracted, and a liquid film model for the split face is established based on the deformation magnitude. Since the liquid film models for Option 1 and Option 2 are similar, only the split face liquid film model for Option 1 is presented below, as shown in Figure 7.

ISSN: 2472-3703 DOI: 10.6911/WSRJ.202601_12(1).0003

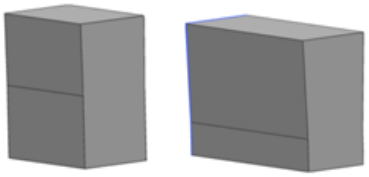

(a) Rotating ring split face (b) Static ring split face

Figure 7. Schematic diagram of the calculation model of the split surface liquid film

(3) Boundary Conditions

In numerical analysis, it is necessary to set the boundary conditions for the liquid film. The boundary conditions for the face liquid film mainly include pressure inlet/outlet boundaries, moving boundaries, and stationary boundaries. A schematic diagram of the boundary condition setup for the seal ring liquid film is shown in Figure 8. The boundary conditions for the remaining liquid film calculation models are similar, with specific operating parameters provided in Table 2.

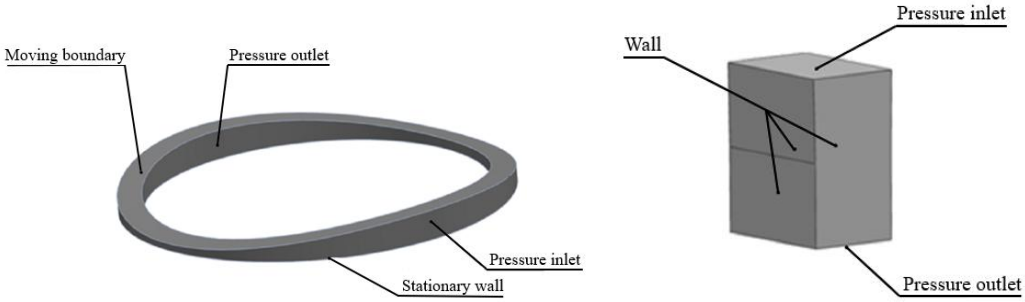

(a) Face liquid film (b) Fluid film on the rotating ring face

Figure 8. Schematic diagram of the boundary conditions of the sealing ring liquid film

Table 2. Working condition parameter table

Parameter	Unit	Value
import pressure	MPa	0.5
export pressure	MPa	0.1
medium (water)	℃	50
rotational speed	rpm	1500
seal face clearance	μm	0.5~3
split face clearance	μm	0.5~3

4. RESULT ANALYSIS AND STRUCTURAL OPTIMIZATION

4.1. Comparison of Leakage Rates

Figure 9 reveals the influence of seal face clearance on the leakage rate of the face liquid film. The leakage rate exhibits a non-linear growth trend with increasing clearance, and the growth rate itself increases as the clearance becomes larger. Under identical clearance conditions, the leakage generated by Option 2 is consistently lower than that of Option 1.

ISSN: 2472-3703 DOI: 10.6911/WSRJ.202601_12(1).0003

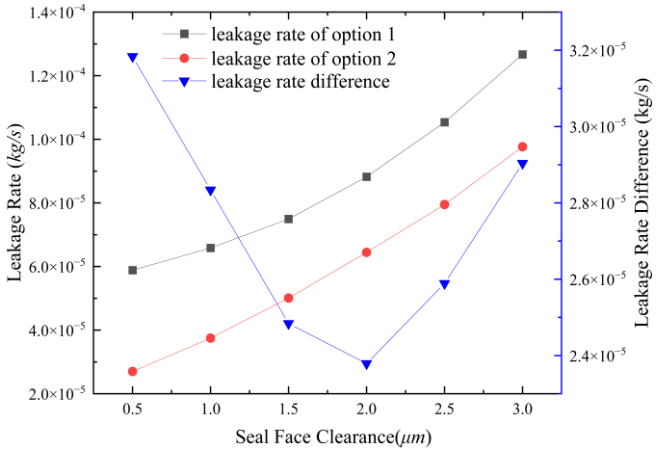

Figure 9. Influence of end gap on the amount of liquid film leakage at the end face

Figure 10 illustrates the correlation between the split face clearance and the liquid film leakage rate. As the split face clearance increases, the leakage rates for both the rotating ring split face and the stationary ring split face in Option 1 gradually increase, with an accelerating rate of growth (Option 2 exhibits a similar trend). At the same split face clearance, the leakage rates for both split faces in Option 2 are slightly lower than those in Option 1.

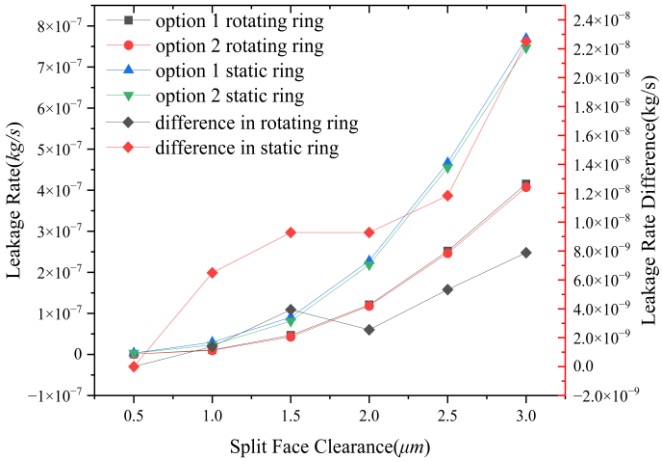

Figure 10. Influence of the profile gap on the amount of liquid film leakage at the profiles

4.2. Structural Parameter Optimization Analysis

The initial basic parameters of the seal rings have been provided in the preceding sections. The key structural parameters analyzed in this subsection are illustrated in Figure 11, and the corresponding dimensional ranges are listed in Table 3.

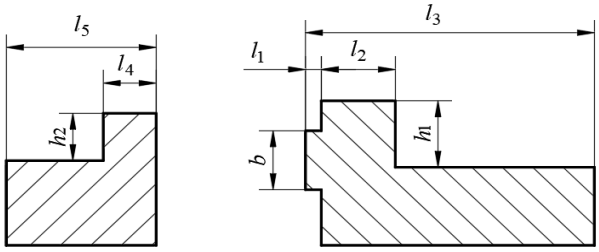

Figure 11. Schematic diagram of the main structural parameters of the sealing ring

ISSN: 2472-3703 DOI: 10.6911/WSRJ.202601_12(1).0003

Table 3. Main structural dimensions range

Parameter	Value (mm)
rotating ring rib thickness l_4	2~4
static ring rib thickness l_2	3.2~5.2
rotating ring rib height h_2	1.85~3.85
static ring rib height h_1	2.2~4.2
static ring face crown height l_1	1~3
static ring face width b	2.55~3.55

The geometric parameters of the seal rings significantly affect the deformation of both the sealing faces and the split faces. Unsuitable structural parameters may lead to increased axial and circumferential clearances, thereby exacerbating leakage. To optimize sealing performance, with leakage rate as the evaluation metric, an orthogonal experimental design was employed for the combinatorial optimization of structural parameters. Each parameter was set at five levels, and the corresponding factor-level table is presented in Table 4.

Table 4. Table of experimental factor levels

Level	Factor					
	A	B	C	D	E	F
1	2	3.2	1.85	2.4	1	2.55
2	2.4	3.6	2.25	2.6	1.4	2.75
3	3	4.2	2.85	3.2	2	3.05
4	3.4	4.6	3.25	3.6	2.4	3.35
5	4	5.2	3.85	4.2	3	3.55

Following a 6-factor, 5-level design, an $L_{25}(5^6)$ orthogonal test table was established to analyze the six parameters: rotating ring rib thickness (A), static ring rib thickness (B), rotating ring rib height (C), static ring rib height (D), static ring face crown height (E), and static ring face width (F). A total of 25 different parameter combinations were analyzed. The leakage results for each scheme are presented in Table 5, where the scheme code consists of a letter representing the factor and a number indicating the corresponding level.

ISSN: 2472-3703 DOI: 10.6911/WSRJ.202601_12(1).0003

Table 5. Table of orthogonal experiments

Test Number	Test Option	Leakage Rate (kg/s)
1	A1B1C1D1E1F1	1.97E-04
2	A1B2C2D2E2F2	1.51E-04
3	A1B3C3D3E3F3	1.07E-04
4	A1B4C4D4E4F4	8.22E-05
5	A1B5C5D5E5F5	5.66E-05
6	A2B1C2D3E4F5	8.42E-05
7	A2B2C3D4E5F1	6.58E-05
8	A2B3C4D5E1F2	1.45E-04
9	A2B4C5D1E2F3	1.16E-04
10	A2B5C1D2E3F4	9.09E-05
11	A3B1C3D5E2F4	1.12E-04
12	A3B2C4D1E3F5	8.51E-05
13	A3B3C5D2E4F1	6.72E-05
14	A3B4C1D3E5F2	5.56E-05
15	A3B5C2D4E1F3	1.24E-04
16	A4B1C4D2E5F3	5.85E-05
17	A4B2C5D3E1F4	1.22E-04
18	A4B3C1D4E2F5	9.24E-05
19	A4B4C2D5E3F1	8.37E-05
20	A4B5C3D1E4F2	6.38E-05
21	A5B1C5D4E3F2	8.56E-05
22	A5B2C1D5E4F3	7.21E-05
23	A5B3C2D1E5F4	4.55E-05
24	A5B4C3D2E1F5	1.01E-04
25	A5B5C4D3E2F1	9.09E-05

In an orthogonal experiment, performing a range analysis of the experimental results is an efficient and intuitive data processing method. It can quickly identify the extent to which different factors affect the evaluation indicators, and based on this, determine the optimal combination of levels for each factor, thereby obtaining the optimal solution in terms of factor combinations. When analyzing with leakage volume as the assessment indicator, the size of the range directly reflects the order of influence of the factor on the leakage volume; the larger the range, the more significant the factor's impact on the indicator. The analysis results are shown in Table 6.

ISSN: 2472-3703 DOI: 10.6911/WSRJ.202601_12(1).0003

Table 6. Leakage Extreme Variance Analysis Table

Level		l_4	l_2	h_2	h_1	l_1	b
K (E-4)	1	5.94	5.37	5.08	5.07	6.89	5.05
	2	5.02	4.96	4.88	4.69	5.62	5.01
	3	4.44	4.57	4.50	4.60	4.52	4.78
	4	4.20	4.39	4.62	4.50	3.70	4.53
	5	3.95	4.26	4.47	4.69	2.82	4.19
k (E-5)	1	11.9	10.7	10.2	10.1	13.8	10.1
	2	10.0	9.92	9.77	9.37	11.2	10.0
	3	8.88	9.14	8.99	9.19	9.05	9.55
	4	8.41	8.77	9.23	9.00	7.39	9.05
	5	7.90	8.52	8.95	9.39	5.64	8.39
R (E-5)		3.97	2.22	1.21	1.15	8.14	1.71
SS (E-10)		50.2	16.6	5.55	3.80	204.0	10.2

According to the range analysis method, the static ring face crown height has the largest R value when leakage is used as the test index. The data in Table 6 were processed using the analysis of variance (ANOVA) method, and the results are presented in Table 7.

Table 7. Leakage ANOVA table

Source of Difference	SS	df	MS	F	Threshold
A	5.02E-9	4	1.25E-9	13.19	
B	1.66E-9	4	4.14E-10	4.35	
C	5.55E-10	4	1.39E-10	1.46	$F_{0.01}(4, 4)=15.98$
D	3.80E-10	4	9.51E-11	1.00	
E	2.04E-8	4	5.11E-9	53.75	$F_{0.05}(4, 4)=6.39$
F	1.02E-9	4	2.54E-10	2.67	
Error	3.80E-10	4	9.51E-11		

Using the smallest term in the sum of squared deviations (SS) as the error term, the F-values were calculated. By comparing these values with the critical values, the order of influence of each factor on leakage was determined as follows: static ring face crown height, rotating ring rib thickness, static ring rib thickness, static ring face width, rotating ring rib height, static ring rib height.

The influence patterns of each factor on leakage are shown in Figure 12. The figure indicates that as the rotating ring rib thickness, static ring rib thickness, static ring face crown height, and static ring face width increase, leakage gradually decreases. Similarly, leakage generally shows a decreasing trend with an increase in rotating ring rib height. Based on the orthogonal experimental results and the influence patterns of each factor on leakage, the optimal structural parameter combination for sealing performance is: l_4= 4 mm, l_2 = 5.2 mm, h_2 = 3.85 mm, h_1 = 3.6 mm, l_1 = 3 mm, b = 3.55 mm, with a corresponding leakage rate of 3.77×10^{-5} kg/s.

ISSN: 2472-3703 DOI: 10.6911/WSRJ.202601_12(1).0003

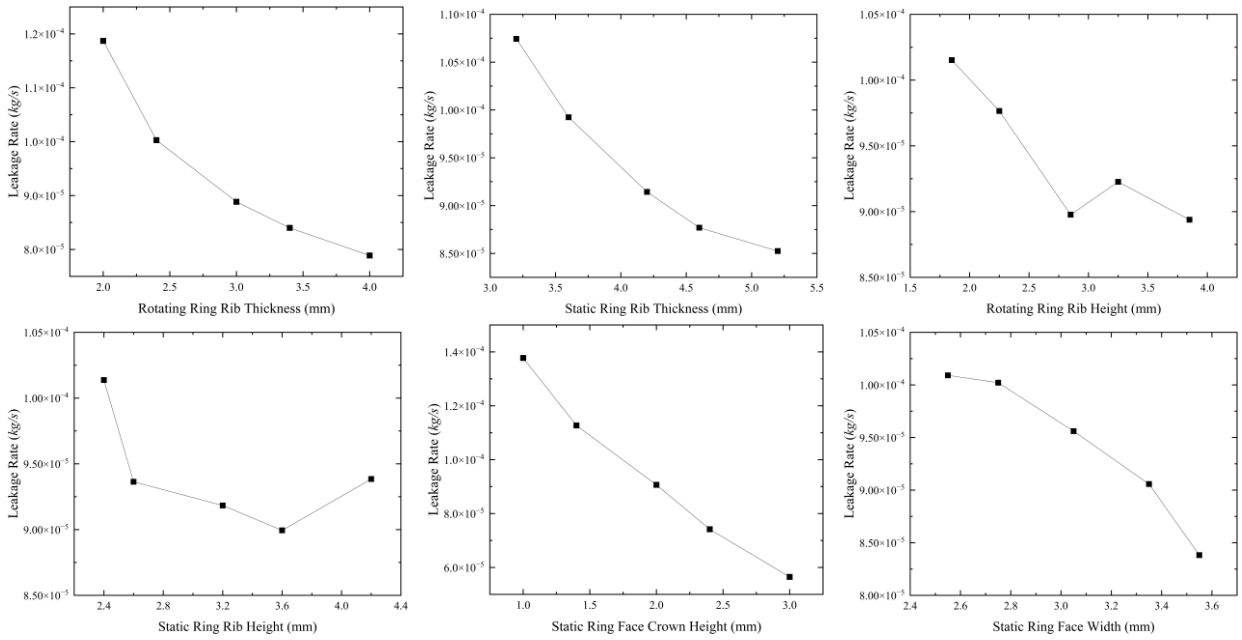

Figure 12. The change rule of the variation of the leakage amount by each factor

5. CONCLUSION

This study proposes a novel split mechanical seal structure (Option 2) featuring a 90° misalignment installation between the sealing ring and its support component. A comparative analysis was conducted with the traditional coplanar arrangement (Option 1), yielding the following conclusions:

(1) The novel split mechanical seal structure proposed in this study exhibits superior sealing performance compared to the traditional split mechanical seal structure.

(2) The seal face leakage increases nonlinearly with the enlargement of the face gap. Under the same gap condition, the leakage in Option 2 is consistently lower than that in Option 1.

(3) As the split interface gap increases, the leakage at the split interface gradually rises. For the same split interface gap, the leakage generated in Option 2 is less than that in Option 1.

(4) Through orthogonal experiments, the order of influence of various structural factors on leakage was determined as follows: static ring face crown height, rotating ring rib thickness, static ring rib thickness, static ring face width, rotating ring rib height, static ring rib height. The optimal combination of structural parameters for sealing performance is: l_4= 4 mm, l_2 = 5.2 mm, h_2 = 3.85 mm, h_1 = 3.6 mm, l_1 = 3 mm, b = 3.55 mm.

REFERENCES

[1] Nagai Yataro, Mitsuyoshi Matsushita, Yuji Yamauchi. Mechanical seal including a split ring: US, 5067733A [P]. 1991-11-26.

[2] Radosav J J, Dudik D M, Brauer Q T, et al. Modular Mechanical Seal: China, 1094139A [P]. 1994-10-26.

[3] Bessette R F, Simmons L K, Proulx G S, et al. Fully split car-tridge mechanical seal assembly: US, 05662340A [P].1997-09-02.

[4] Reagan MP. Split face mechanical sealing rings and their use: US, 05615893A [P]. 1997-04-01.

[5] Giard B. Mechanical seal assembly: US, 2007267818 [P]. 2007-11-22.

[6] Boyson S. Reliability performance of split seal technology when combined with a centrifugal flow device [J]. Sealing Technology, 2007 (7) :7-10.

ISSN: 2472-3703 DOI: 10.6911/WSRJ.202601_12(1).0003

[7] Ma Weidong. Split-type mechanical seal: China, 2378578Y [P]. 2000-05-17.

[8] Li Zhenhuan, Li Yan. Design Characteristics and Applications of Division Seal Structures for Boilers [J]. Fluid Machinery, 2002, (01):42-43.

[9] Shao Jiaxing, Yao Liming, Li Kun, et al. Analysis of Mechanical Seal Structure for Fully Split Kettles [J]. Fluid Machinery, 2003, (08): 36-38.

[10] Zhang Yuan, Yang Qiming. Design of a New Split-Type Mechanical Seal Device for Kettles [J]. Chemical Machinery, 2009, 36(02):96-99.

[11] Chen Bifeng. Finite Element Analysis of Split Mechanical Seal Structure [J]. Machinery, 2010, 37(09): 34-36.

[12] Wang Hongqun, Yu Peiqing. Fully split mechanical seal for kettles: China, 101725712A [P]. 2010-06-09.

[13] Tao Kai, Tu Qiao'an, Sun Jianjun, et al. Deformation Analysis of Split Mechanical Seal Based on ANSYS [J]. Lubrication & Sealing, 2014, 03:84-90.

[14] Feng Feifei, Yang Qiming, Mao Dongbi, et al. Analysis and Study of Split Mechanical Seals [J]. Mining Machinery, 2015, 43(02): 5-8.

[15] Hu Qiong, Sun Jianjun, Tu Qiaoan, et al. Research Status and Key Issues Exploration of Split Mechanical Seal Technology [J]. Progress in Chemical Industry, 2015, 34(05): 1207-1214.

[16] Liang Xiao, Zhu Weibing, Wang Fenglin, et al. Failure Analysis and Improvement of Split Mechanical Seals for Kettles Based on FMEA [J]. Lubrication and Sealing, 2025, 50(02): 170-177.